CrossMark

ORIGINAL PAPER

Integrated geo-scientific surveys in the historical centre of Mesagne (Brindisi, Southern Italy)

G. Leucci[1] · L. De Giorgi[1] · F. T. Gizzi[2] · R. Persico[1]

Abstract The topographic and geo-morphological characteristics of the Salento peninsula (Puglia, south-eastern Italy) mean that movements of mass are extremely rare. These phenomena particularly affect certain coastal zones characterized by cliffs in rapid retreat and some unusual points in the hinterland in which collapses, generally linked to the development of karstic cavities, are common. These phenomena demonstrate the brittleness of some areas of the Salento, and they constitute a restraint on the use of the territory itself. The town of Mesagne is one of the sites at greatest geological risk in the north Salento peninsula. In the last few decades, the historical centre of Mesagne has been affected by a series of subsidence events, which have, in some cases, resulted in the partial collapse of buildings and road surfaces. The last event was in the January 2014. It caused subsidence phenomenon in a wide area, and many families have been forced from their homes. These events have had both social repercussions, causing alarm and emergency situations, and economic repercussions in terms of the expense of restoration. In order to determine the causes of the ground subsidence events, integrated geophysical surveys were undertaken in the historical centre of Mesagne. In addition, the analysis of several wells allowed the 3D model reconstruction related both to the geology and to the groundwater depth in the surveyed areas. With the purpose of estimating the dimensions of the phenomenon and its possible relationship with both specific environmental conditions (for instance groundwater depth variation) and anthropic conditions (for instance the losses in water supply and sanitation), some geophysical measurements were repeated in the time. The study led to the production of a detailed description of the subsidence causes that allows a quick action to restore security conditions in the area.
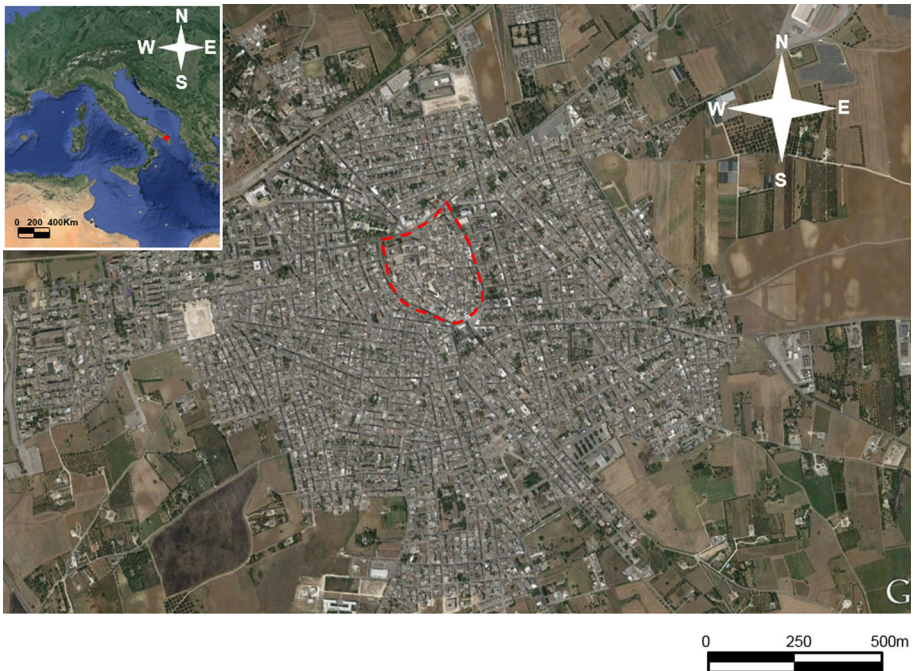
✉ G. Leucci
  g.leucci@ibam.cnr.it

[1] Institute for Archaeological and Monumental Heritage (IBAM), National Research Council (CNR), Lecce, Italy

[2] Institute for Archaeological and Monumental Heritage (IBAM), National Research Council (CNR), Potenza, Italy

1 Introduction

Geophysical methods play an important role within many important applications. In particular, it is an important non-invasive technique widely exploited in the contexts of discovery and/or preservation of cultural heritage (Giannotta et al. 2015; Goodman and Piro 2013; Leucci et al. 2011; Leucci 2015) and civil engineering (Cataldo et al. 2014; Piscitelli et al. 2007; Gallipoli et al. 2012), that are the most relevant for this contribution. Other authors use ERT and GPR to study the subsidence related to the karst phenomena (Capizzi et al. 2012; Carbonel et al. 2014, 2015; Tsokas et al. 2015). In some cases, the two kind applications can converge together, as e.g. in the case of the investigation of columns (Leucci et al. 2007). In this paper, these two kind of interests are joined together. In particular, a multisensory measurement campaign will be presented, including earth resistivity tomography (ERT), self-potential (SP), and ground penetrating radar (GPR) investigations carried out in the historical centre of Mesagne, placed in the Apulia region near Brindisi, Southern Italy (Fig. 1). In particular, after a strong storm a pipe of the aqueduct in Mesagne broke down causing serious subsidence events. Fortunately, no person has been injured during the event, but several buildings have been seriously damaged, and the local municipality has been compelled to vacate several houses that have become definitely dangerous after the event. Moreover, the municipality of Mesagne

Fig. 1 Town of Mesagne (Apulia Region, Italy), with its historical centre (shown with *broken line*)

contacted the Institute for Archaeological and Monumental Heritage IBAM-CNR and committed a non-invasive geophysical measurement campaign in order to provide some insight with regard to the entity and extension of the damages within a part of the old town. The results of these investigations were particularly important because the municipality had to establish whether some tens of people could come back to their houses, or rather they should look for alternative solutions. In particular, the municipality had provided provisional accommodations to several people, which was of course a meaningful cost for them. The situation was made somehow even more complicated by the fact that, indeed, several artificial cavities are present under the houses of the historical centre of Mesagne, due to a number of cisterns (whose dating is quite uncertain and variable from case to case, but the most ancient ones are thought to be many centuries old) reused in several ways during subsequent periods (included the exploitation as waste containers) and then definitely abandoned in the twentieth century and in most cases currently corked. Indeed, in many cases also the memory of the presence of these structures is lost, because the houses changed ownership several times. In particular, the old town of Mesagne was inhabited by the Messapic people since sixth-century BC Then, the town passed through the Roman, Greek-Byzantine, Norman, Svevian, French, and Spanish dominations that left traces of great historical and artistic value on which, however, the inevitable effects of anthropogenic modifications are evident. In particular, it is probable that important remains are still hidden under the soil, because still in 1999 Messapic tombs dating back to the fifth century BC were found (Leucci and Negri 2006).

The old town was also affected by significant morphological changes because of occurred levelling, excavations and subsequent debris flows, as it is put into evidence by several documents in the archives of the technical office of the municipality of the town. The geology of the historical centre and more in general of the town of Mesagne is characterized in the first metres by the presence of clayey weakly cemented sands. The water table is located at an average depth of about 4 m from the current living surface level. In particular, the geological substrate, formed by sands, is affected by some degradation processes in its superficial parts whose most significant effect is the gradual removal of the cemented part of the subsoil, due to the rainfall and to the meaningful amount of dropped water from the supply networks and from the drainage systems. Indeed, these degradation processes caused in the old town centre of Mesagne several documented subsidence events also in the past so that the town was included among the Apulia sites at risk of cavity collapse (Leucci et al. 2002; Autorità di Bacino della Puglia 2006).

In order to probe the current event, an integrated ERT, SP and GPR prospecting was performed, showing one more time the capabilities of the non-invasive techniques in identifying, within the first metres of depth, a number of anomalies, partially ascribable to collapses and of cavities.

Furthermore, using stratigraphical information related to 17 wells in the historical centre, a 3D model related to geology and ground water was performed.

1.1 Geographic and regional geological settings of the study area

Mesagne town is located near Brindisi, in the northern part of the narrow and flat Salento peninsula, an area at the southern end of the Apulia region, in Southern Italy (Fig. 1). The *peninsula* has *the Adriatic* Sea to the east, the *Ionian Sea* to the west and the Murge hill to the north. From a geological point of view, the Salento carbonatic continental shelf is a portion of the Apulian stable foreland of the Southern Apennines chain (Cinque et al. 1993).
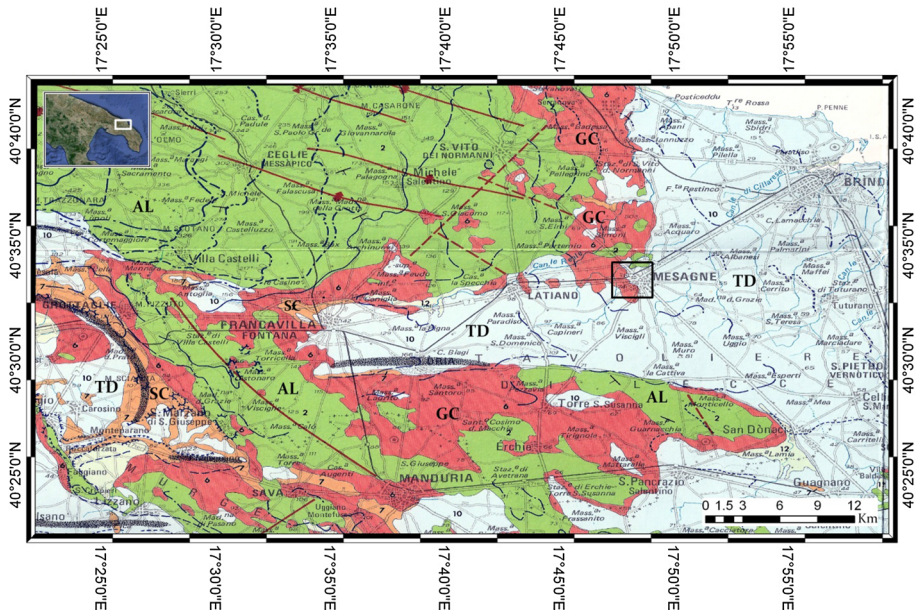
Fig. 2 South-West Brindisi Provincia geological map; (after Ciaranfi et al. 1992, modified). *AL* Altamura Limestone (cretaceous); *GC* Gravina Calcarenite (Lower Pleistocene), *SC* Subapennine Clays (Lower Pleistocene); *TD* Terraced Deposits (Middle–Upper Pleistocene) (Ciaranfi et al. 1992)

Taking the regional scale in mind and looking at the lithological features, four are the main formations that outcrop in the northern Salento area: the Altamura Limestone (Cretaceous), the Gravina Calcarenite (Lower Pleistocene), the Subapennine Clays (Lower Pleistocene) and the Terraced Deposits (Middle–Upper Pleistocene) (Ciaranfi et al. 1992) (Fig. 2).

The Altamura Limestone, that outcrops to the north–west and south of Mesagne, is made up of alternating layers of limestone and dolomitic limestone. The formation, that reaches several thousand of metres in thickness, makes up the bedrock of the whole Apulia region and hosts the most important deep aquifer of the Salento peninsula (Giudici et al. 2012).

The Gravina Calcarenite, that is made up of bio-detritic calcarenite overlaying the Altamura Limestone transgressively, outcrops to the west, to the north and in a large area to the south of the site under investigation.

The Subapennine Clays formation, constituted by grey-blue clay and silt, outcrops in narrow areas to the west of Mesagne.

The last formation of the area is represented by the transgressive Terraced Deposits that outcrop widely in the northern portion of Salento. The sediments are constituted by yellowish quartzitic sands and bio-calcarenites that, on the whole, host a shallow aquifer due to the presence of the underlying impermeable Subappennine clays deposits.

1.2 The problems of the study area

As said before, the Terraced Deposits form the soil on which Mesagne historical centre lies. Locally the outcropping soil is made up of poorly cemented clayey sands. As concerns

the aquifer, the shallow water table is located at an average depth of about 4 m from the ground level. The surveyed site is generally affected by hydrogeological subsidence caused by the:

1. Variability of the level of the superficial water table (from about 3 to about 5 m in depth);
2. Losses of the old water pipes and drainage system;
3. Uncontrolled drawing from numerous wells;
4. Presence of man-made and natural cavities.

These are the main causes of the static trouble of some buildings. In fact the geological substrate is constituted by sands of the transgressive Post-Calabrian units, which are mainly melted and affected by degradation processes in their most superficial parts. The main aspect of this degradation process consists in the progressive carrying away of the cementing part under the influence of the water table and rain water. The conditions of the hydrogeological hazard, characterizing the subsurface of Mesagne, depend essentially on the upper level variations of the almost superficial water table.

The main negative effects can be summarized by two points:

• Washing away and progressive degradation of foundational structures;
• Damage of water supply and drainage pipes, particularly prone to dangerous breaks without constant and effective maintenance.

This last point is very important because it concerns the direct leaking of water into the subsurface. The water network losses are certainly more dangerous than the natural infiltration, because of their continuous and concentrated action near the broken pipe zone. In the historical centre of Mesagne many buildings have developed several cracks (Fig. 3)
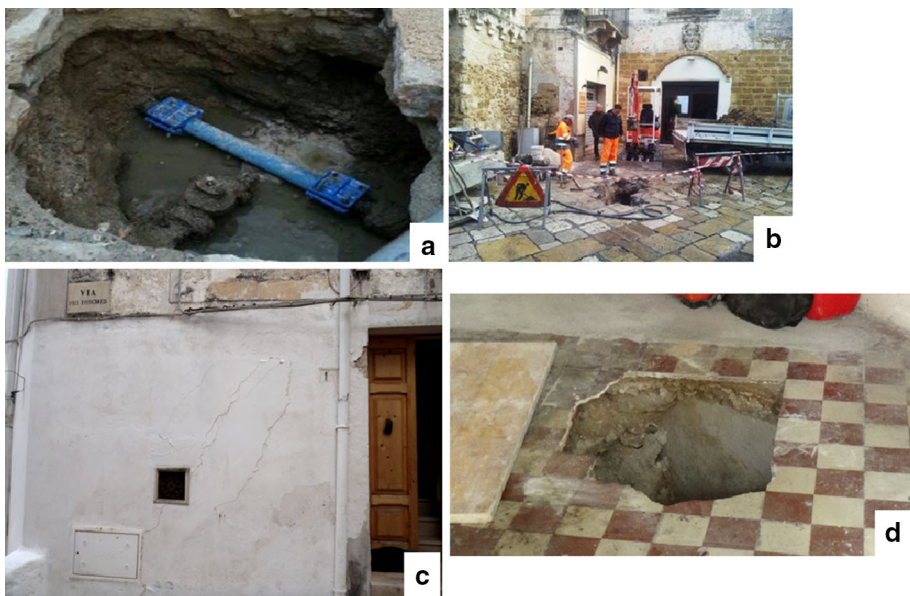
Fig. 3 Photograph of some problems at some buildings in the historical centre. The photographs show the water pipe loss (**a**); the intervention of the Apulian aqueduct technical at the point loss (**b**); the crack on the wall near the loss point (**c**); the cavity inside the dwelling near the point loss (**d**); (photographs by Leucci)

caused by hydrogeological subsidence and losses from the water network. Once the break in the pipe had been repaired, a non-invasive investigation of the whole area was proposed to establish other possible losses.

2 3D models

Using the software Groundwater Modeling System (GMS) a 3D geological model, containing lithological information, and a 3D groundwater model, containing water flow velocity, ground water thickness, and water flow direction, were performed. The scope of building a model is to simplify the field problem and organize the field data so that the system can be analysed more readily (Anderson and Woessner 1992). The conceptualization of the model includes synthesis and framing up of data pertaining to geology, hydrogeology, hydrology, and meteorology. The lithologic data were collected from 17 lithologs of drinking-water whose location is shown in Fig. 4. Based on the acquired lithologs, a lithologic model was developed with Groundwater Modeling System (GMS). The lithologic solid model was created using a block-centric finite-difference grid. The gridding was performed through the eight nearest-neighbour methodology with 3D interpolation by average minimum distance. The solid model was developed to a depth of about

Fig. 4 Location of the 17 analysed wells

20 m b.g.l. The sensitivity of the model was tested by varying the horizontal and vertical spacing of the nodes, and an optimized final model, least sensitive to changes in spatial resolution (i.e. smaller grid sizes), was built. The resolution of the final model was 1 m × 1 m × 0.2 m. The resulting discretization consisted of 250 nodes × 250 nodes × 100 nodes, obtaining 6,250,000 solid model nodes, each with a voxel volume of 20,000 m^3. It should be noticed that the results of the modelling are not free from uncertainties, which could be reduced by increasing data points number, but they illustrate one of the most probable scenarios. The smallest scale of variation that the model is able to depict is equal to the resolution of one voxel. Given the heterogeneity and complexity associated with the study area (e.g. local-scale variations of aquifer properties), some generalizations, simplifications, and assumptions were made to construct the groundwater flow model. The 3D constant-density groundwater flow was simulated by a block-centric, finite-difference grid model, using MODFLOW code inside GSM software. Furthermore, MODAEM code, which allows the analysis to the analytical elements (polygons, lines, and points), was used. MODAEM was used to extract information related to the depth and thickness of the aquifer inside the area under investigation. The study area was horizontally discretized in the same way as described in the above paragraph. The maximum thickness of the model was 20 m. The model was vertically discretized in four layers. The layers had variable thickness as a result of wells stratigraphy. The layers were allowed to have seepage from the top and leakage through the base, making them hydraulically connected. The top-most layer and the second layer were defined as unconfined. The rest of the layers were defined as confined, as the water table was not expected to fall >10 m (Leucci et al. 2003). The conductivity was assigned to layers according to the modelled lithology. Vertical hydraulic conductivity (kz) was ranging from 0.86 to 0.64 m/d for the various types of calcarenite present in the study area and ranging from 2×10^{-2} to 0.8×10^{-2} m/d for the limestone (Sileo 2011). Other parameters were the horizontal anisotropy, the vertical anisotropy, the effective porosity, and the porosity. What concerns anisotropy ratio is related to hydraulic conductivities in different directions. For example, vertical to horizontal hydraulic conductivity anisotropy ratio is given by kr/kz, where kz is the vertical hydraulic conductivity and kr is the radial (horizontal) hydraulic conductivity. Anisotropy in a horizontal plane is given by kx/ky where kx and ky are horizontal hydraulic conductivities in the x and y directions, respectively. In the case of the study area, hydraulic conductivity kx ranges from 0.36 to 0.067 m/d and for the various types of calcarenite present, and it ranges from 0.025 to 0.032 m/d for the limestone (Sileo 2011), while ky ranges from 0.31 to 0.054 m/d for the various types of calcarenite present, and it ranges from 0.013 to 0.018 m/d for the limestone (Sileo 2011). Consequently, the horizontal anisotropy ranges from 1.16 to 1.24 for the various types of calcarenite present in the study area, and it ranges from 1.92 to 1.78 for the limestone. On the other hand, the vertical anisotropy ranges from 0.39 to 0.094 for the various types of calcarenite present and from 0.95 to 0.31 for the limestone. The total porosity is defined as the fraction of the bulk rock volume V that is not occupied by solid matter. It should be noticed that the porosity does not give any information concerning pore sizes, their distribution, and their degree of connectivity. Thus, rocks characterized by the same porosity could have widely different physical properties. An example of this might be a carbonate rock and a sandstone. Each could have a porosity of 0.2, but carbonate pores are very often unconnected resulting in its permeability being much lower than that of the sandstone. There is also an "effective" porosity defined as the ratio between the connected pore volume and the total volume (Juhasz 1986, Hill et al. 1979, Clavier et al. 1977). The most common definition of "effective" porosity is (Juhasz 1986, Hill et al. 1979, Clavier et al. 1977):

$$Fe = Ft - VD, \tag{1}$$

where Ft is the total porosity of clean (clay free) sand, and VD is the volume of dispersed clay in the sand pore space expressed as a fraction of the bulk volume.

Sileo (2011) has performed experimental studies on the hydrological characteristics of the calcarenite, some of which are present in the study area, and she has found that the "effective" porosity ranges from 27 to 45%, while the total porosity ranges from 32.4 to 54%. No detailed previous data on the total recharge were available for the study area, and hence, it was one of the least certain input parameters. The total recharge inflow in the study area can be estimated on the basis of a fundamental source related to the precipitation. In particular, the average annual precipitation was calculated using multiple year data (about 80) for six locations in and near the study, and it is 649.4 mm (Leucci et al. 2003). The total water from rain available for recharge can be termed as potential recharge (PR) and is defined as follows:

$$R - ET = PR = AR + SF, \tag{2}$$

where R is the total precipitation, ET is the evapotranspiration, SF is the surface overflow, and AR is the amount of meteoric water that actually recharges the aquifer. Accurate quantification of AR and SF requires long-term hydraulic head data and surface water stage measurements from multiple locations in the study area. Because such data were not available, AR was estimated indirectly by approximation of seasonal PR from meteoric data (80 years). The PR was estimated as a difference of the total precipitation and the ET in a specific area. ET was calculated by the method of Pike (1964) as:

$$ET\,[\text{mm/month}] = \frac{P}{\left[1 + \left(\frac{P}{PET}\right)^2\right]^{1/2}} \tag{3}$$

where P is the average precipitation [mm/month], and PET is the potential evapotranspiration [mm/month]. Values of PET were approximated from the method of Malmström (1969):

$$PET\,[\text{mm/month}] = 40.9 \cdot K \cdot \tau, \tag{4}$$

where $k = 0.611 \exp (17.3\,\tau/\tau + 237.3)$ and τ is average monthly temperature (°C). The average PR calculated for the study area is 266 mm/year equal to 41% of the mean annual rainfall. These calculated PR data were used to develop zonal recharge values by kriging them in the seasonal flow models. In the studied area, hydraulic heads in observation wells ($n = 17$) fall in the range between 0.5 and 0.7 m because of nonextensive pumping. This indicates that the total annual recharge is equal to the difference in groundwater levels between wet and dry seasons.

The lithologic modelling suggests the presence of a very complex 3D hydrostratigraphic framework in the subsurface of the studied area. A detailed description of the study area at the block scale is provided here to illustrate the general spatial trends in aquifer thickness and spatial variability. According to the regional geological features of the Salento peninsula, 3D model (Fig. 5) with the cross sections (Fig. 6) provides detailed depictions of the lithology of the studied area.

Figure 7 shows the groundwater depth level referred to the living surface. As expected, the ground water level ranges between 1 and 5 m. In the south part of the historical centre, a greater depth of groundwater level is seen. In this zone, groundwater depth is at about
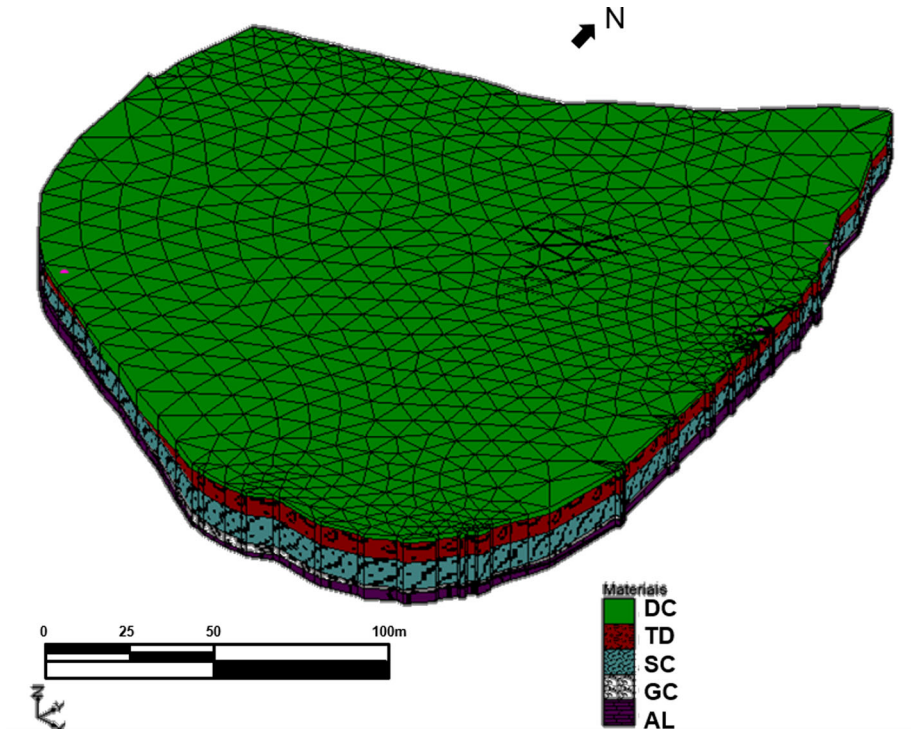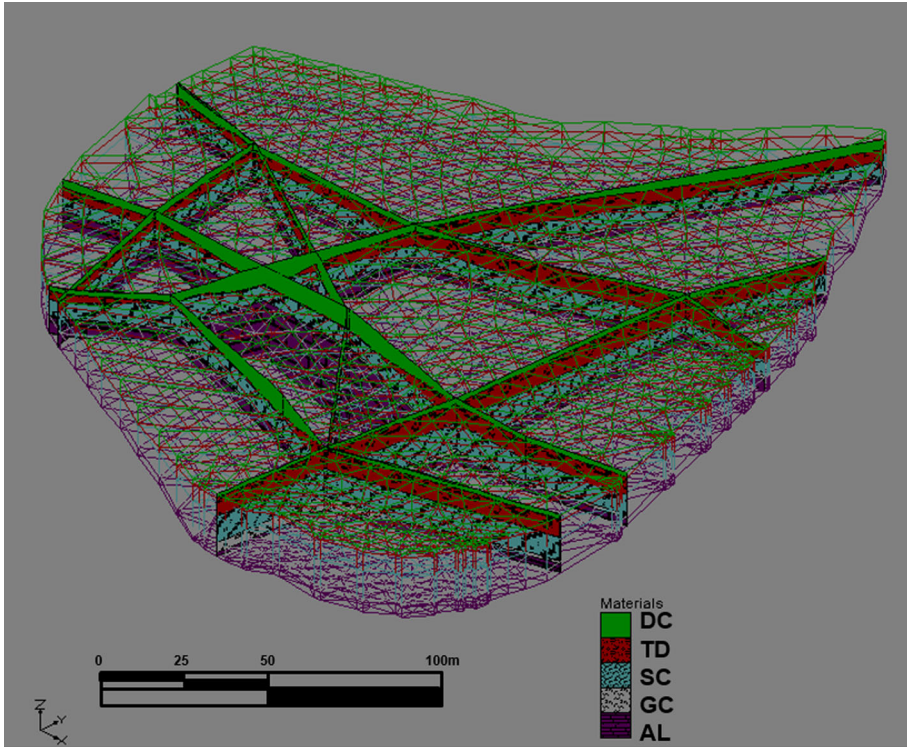
Fig. 5 3D lithological model: *DC* debris covers; *AL* Altamura Limestone (Cretaceous); *GC* Gravina Calcarenite (Lower Pleistocene), *SC* Subapennine Clays (Lower Pleistocene); *TD* Terraced Deposits (Middle–Upper Pleistocene)

5 m b.s.l. The velocity flow model (Fig. 8) suggests that it was topographically controlled. The groundwater flow velocity ranges from 5×10^{-8} to 14.5×10^{-8} m/s, and its direction is essentially from the centre of the area to the north-west.

2.1 3D ERT data analysis

The surveyed area is approximately 3500 m^2 (Fig. 9). In the area several selected buildings are marked in black in Fig. 9. Therefore, in order to investigate below the buildings, a special ERT arrays were used. The electrodes are distributed in such a way as to surround the buildings (Chavez et al. 2011; Argote-Espino et al. 2013; Tejero-Andrade et al. 2015). A dipole–dipole equatorial-parallel array was used. Initially, a 2D survey is conducted along each perpendicular line or transect. In the next step, the current electrodes remain at the end of one line, while the potential is moved, along the line. Then, the current electrodes move one electrode position and the potential electrodes move as previously described. The process is repeated until the current and potential electrodes cover the L geometry. This sequence of observations produces a series of apparent resistivity observations towards and beneath the central portion of the array. The coloured circles in Fig. 10 represent the attribution points, where the apparent resistivities are measured, for the performed ERT array. This process is discussed in detail by Tejero-Andrade et al. (2015).

Fig. 6 Lithological cross sections: *DC* debris covers; *AL* Altamura Limestone (Cretaceous); *GC* Gravina Calcarenite (Lower Pleistocene), *SC* Subapennine Clays (Lower Pleistocene); *TD* Terraced Deposits (Middle–Upper Pleistocene)

Several L-arrays can be combined to surround a structure to build a 3D matrix of observations.

Resistivity data were collected using a Syscal kid swich device (IRIS Instruments, France) supporting 24 electrodes with two reels of 55-m long connecting cable with 5-m maximum separation between electrodes. The electrode separation for all arrays was 2 m. Cables and electrodes were deployed along the small street around the buildings and subdivided in three profiles labelled, respectively, ERT1, ERT2, and ERT3 (Fig. 11). A penetration depth of 6 m was obtained using a total of 72 electrodes deployed within the boundaries of the studied area. After the data acquisition process was performed, the apparent resistivity data were analysed to identify abnormal measurements with a high standard deviation.

The investigated volume was computed using the software ErtLab (http://www.geostudiastier.it) that makes use of Finite Elements algorithm. The true resistivity model computed has an investigation depth of 6 m, which guarantees that the inverted true resistivity model is deeper than the expected building foundations. The foundations have an expected depth between 1 and 2 m such revealed the GPR results. Several horizontal slices were analysed to observe the extension at depth of the resistivity features. Figure 12 shows the slices from 0.5 to 4.0 m in depth.

At first it is possible to note the presence of a heterogeneous subsurface with resistivity values ranging from 50 to 500 O m^{-1}. Afterwards, it is possible to note the presence of:
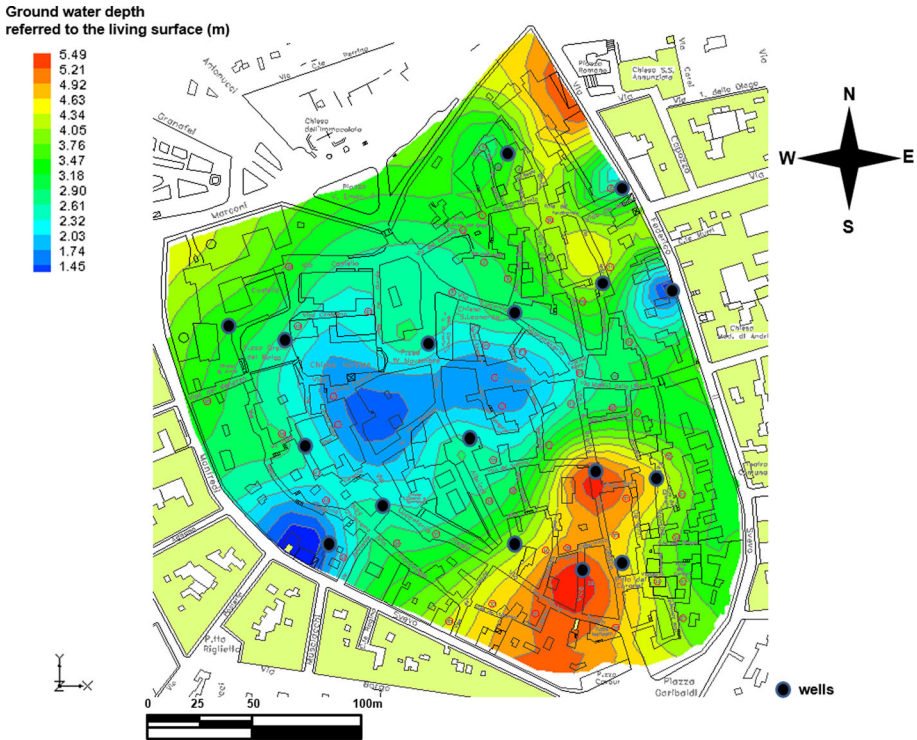
Fig. 7 Ground water depth level referred to the living surface

1. areas indicated with "A", with resistivity values between 400 and 500 O m^{-1}; these values indicate the probable presence of areas where localized phenomena of instability are present. The relatively low resistivity values indicate that these anomalies are not attributable to the presence of empty volumes, but rather to incoherent materials, probably put there in order to fill up previous voids;

2. areas indicated with "B", with resistivity values between 50 and 100 O m^{-1}; these values indicate the probable presence of areas where a phenomenon of instability is present too. The low resistivity values indicate that these anomalies are due to the potential presence of water saturated incoherent materials;

3. areas with resistivity values between 150 and 280 O m^{-1}; these values indicate the probable presence of subsoil zones free of in-homogeneities.

2.2 SP data analysis

The self-potential (SP) method is based on measuring the natural direct current potential between any two points on the ground (Telford et al. 1990). The potential differences are partly constant and partly fluctuating and are associated with electrical currents in the ground. Large anomalous potentials are often observed over sulphide and graphite ore bodies, magnetite and several other electrically conductive minerals (Lowrie 2007), and groundwater accumulations (Meiser 1962, Paul 1965). Self-potential anomalies are also associated with water in subsurface structures and flow of water through the ground
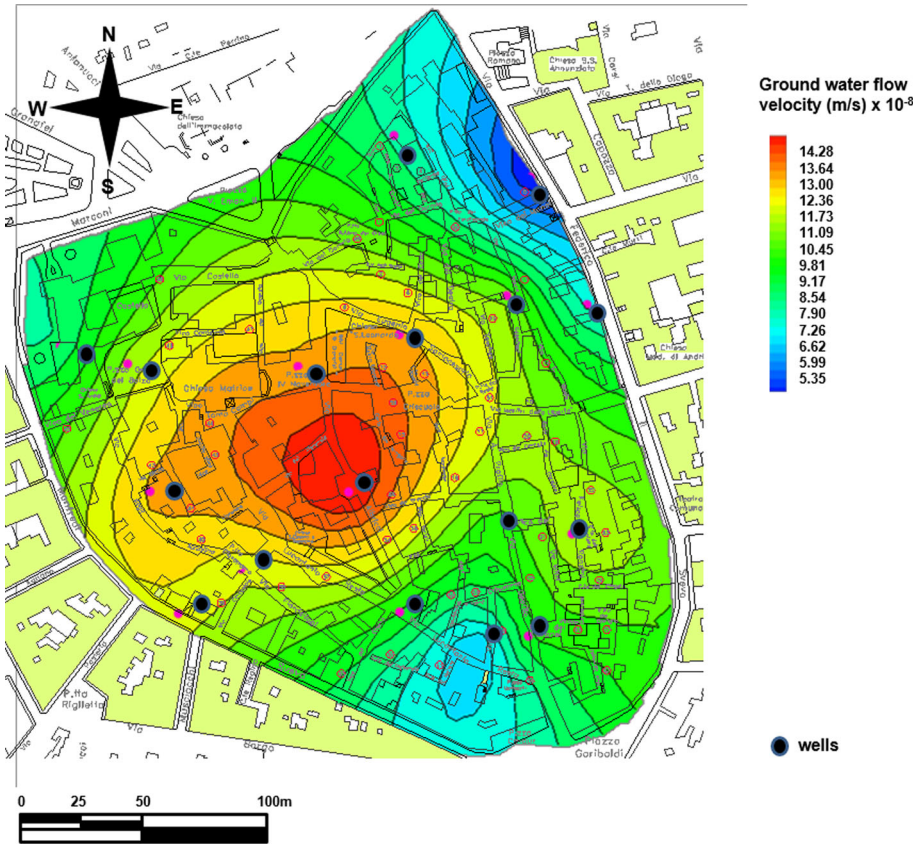
Fig. 8 Ground water velocity flow

(Fig. 13). The streaming self-potential of groundwater is usually indicated as a negative anomaly in the profile (Colangelo et al. 2006). Figure 13 represents horizontal groundwater flow (from right to left), which generates SP data as a linearly increasing line in the direction of flow. The slope of the line is a relative measure of the driving hydraulic gradient (Vichabian and Morgan 2002).

The SP measurements covered the 3D ERT surveyed area. The self-potential signals were measured at the ground surface in a set of 432 measurement points located along the same ERT lines. Each electrode (stainless and non-polarizing) was placed inside a 10-cm bucket, filled with a moistened bentonite and gypsum mixture to ensure good contact between the electrode and the ground. Measurements of the self-potential signals were taken with the same syscal kid, and non-polarizing Pb/PbCl$_2$ (Petiau) electrodes (Perrier et al. 1997) were used. The SP data were filtered with a low-pass filter in the frequency domain in order to avoid edge effects of space domain filters, so that high frequencies were eliminated and low frequencies were preserved (Aubanel and Oldham 1985). These data are used to build self-potential maps shown in Fig. 14. It is important to note that the water flow direction is from negative to positive values of self-potential

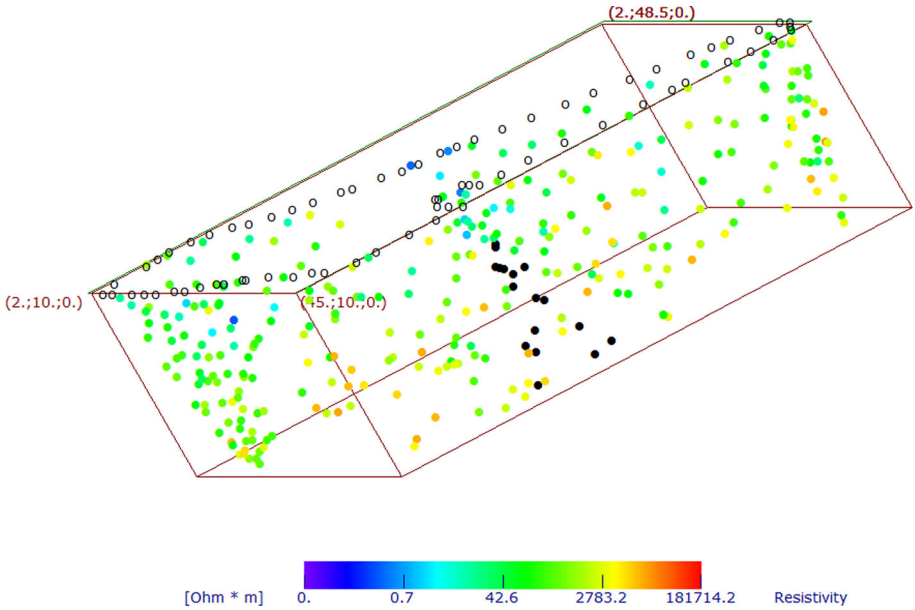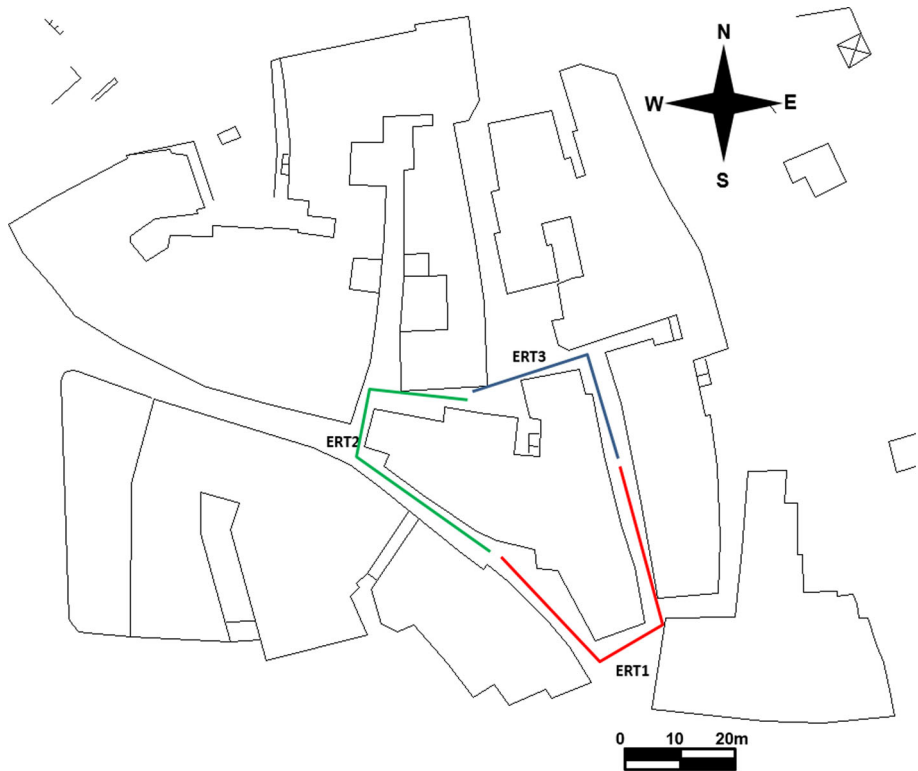**Fig. 9** Geophysical surveyed area

Fig. 10 Apparent resistivity measured points. *White circle* represents the electrode location; *black point* represents bad data

(Fig. 13). The result of this research shows that the self-potential values vary between −10 and 100 mV.

Fig. 11 ERT profiles location

In Fig. 14 a quite uneven distribution pattern of the self-potentials is clearly visible. In particular, it is possible to note two points, indicated with "R", where there is a negative concentration of the spontaneous potential (-10 mV). It is quite probable that, in these points, a flow of waterborne materials, in the directions indicated by the arrows (that is, towards positive SP values) was occurring at the moment of the measure (March 2014).

2.3 GPR data analysis

A large GPR survey was performed too. In order to carry out it, a pulsed RIS Hi Mod GPR system, manufactured by the Ingegneria dei Sistemi IDS-Corporation was used. The system is equipped with a dual-band antenna with central frequencies at 200 and 600 MHz, although only the results from the high-resolution 600 MHz survey are presented here. In particular, the main targets looked for were subservices and cavities, because possibly related to the present or to future subsidence events. So, the targets looked for were expected to have a size between 0.5 and 2 m, and their depth was expected variable from tens centimetres to a few metres.

GPR survey was undertaken both outside and inside the dwellings. The most damaged dwellings were considered. Comprehensively, 174 Bscans, covering an overall surface of about 964 square metres, were acquired.

In order to obtain a 3D model of the subsurface, one should make an adequate field acquisition; consisting of a grid of GPR lines. Hence, several rectangle areas with 0.3 m
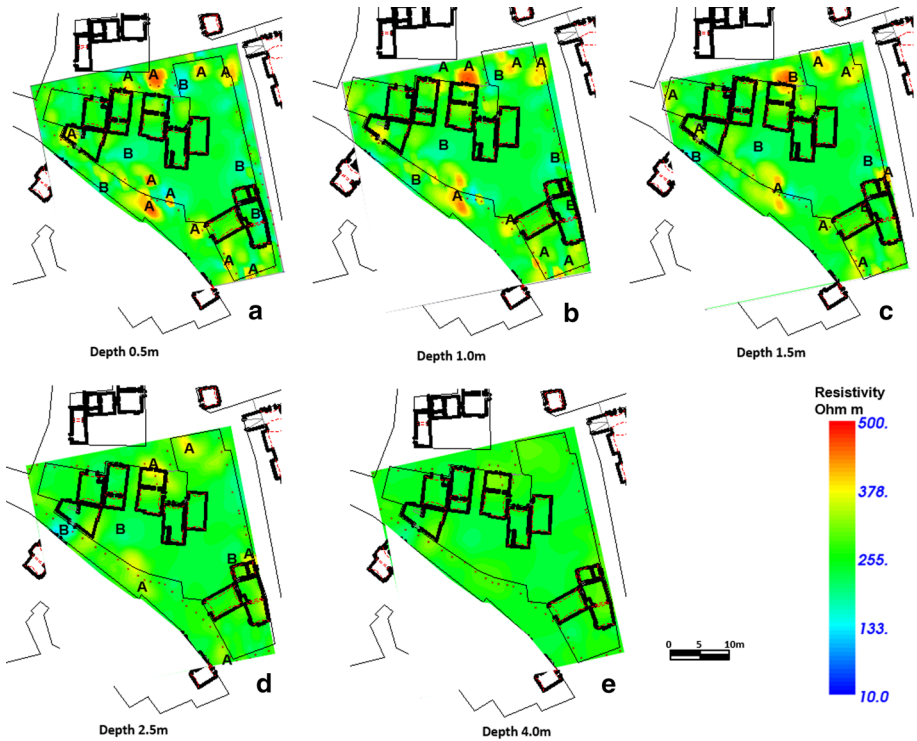
Fig. 12 ERT depth slices: **a** 0.5 m depth; **b** 1.0 m depth; **c** 1.5 m depth; **d** 2.5 m depth; **e** 4.0 m depth
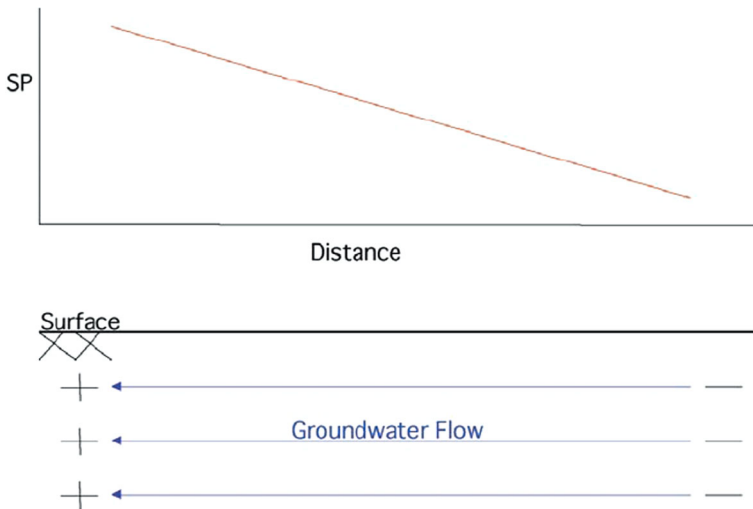

Fig. 13 Schematic response of self-potential distribution in the subsoil with associated water flow

spaced parallel profile were surveyed. The data were subsequently processed using standard two-dimensional processing techniques by means of the GPR-Slice Version 7.0 software (Goodman 2013). The processing flow chart consists of the following steps: (1)
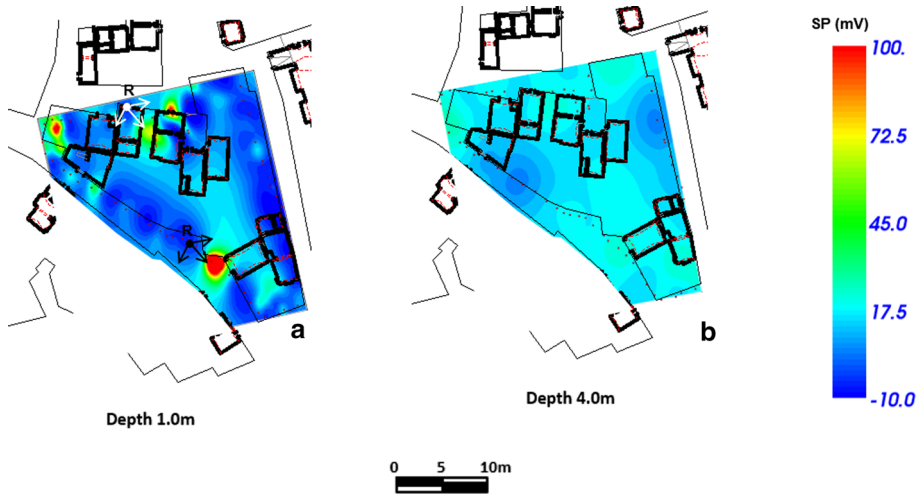
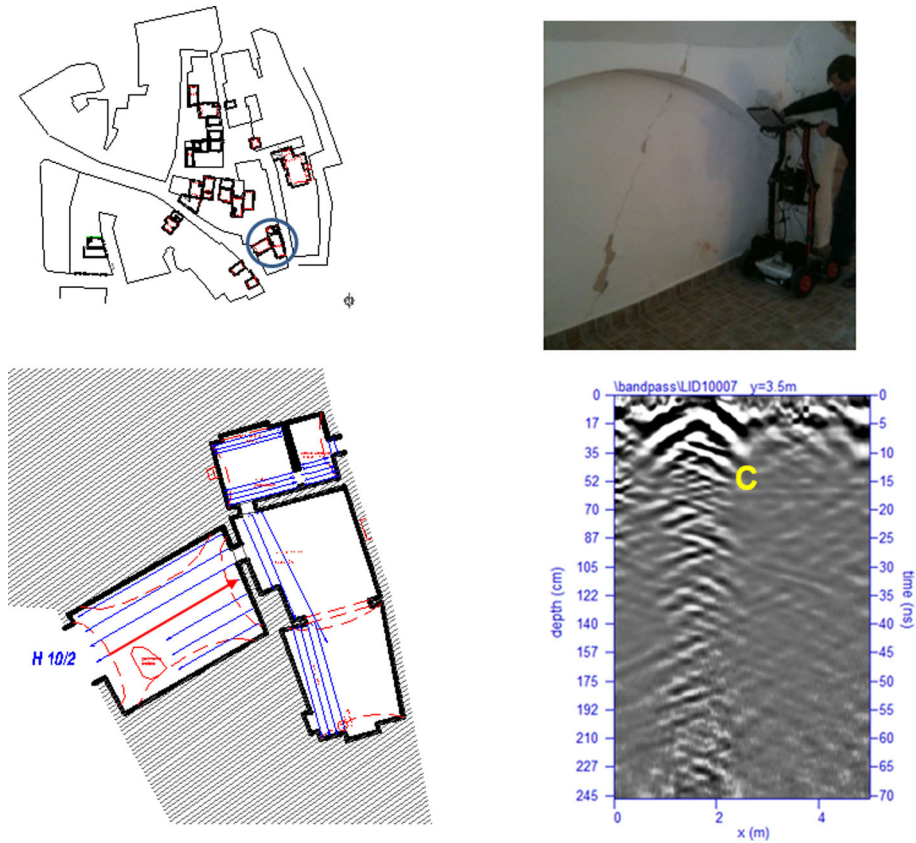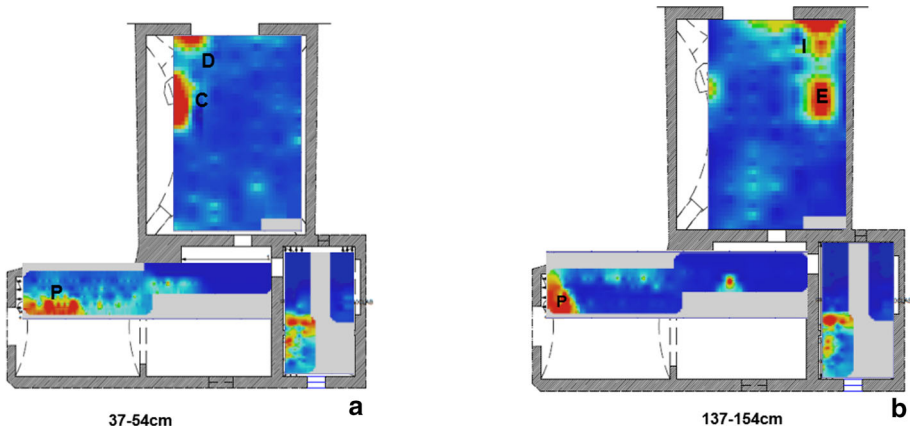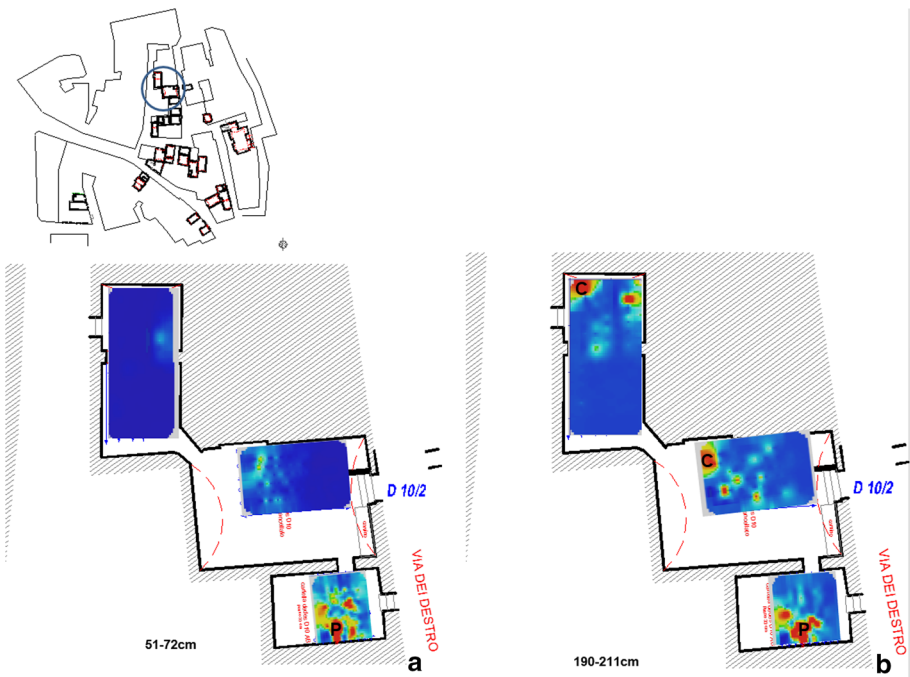**Fig. 14** SP depth slices: **a** 1.0 m depth; **b** 4.0 m depth

Fig. 15 Processed radar section related to one of the profiles (*red arrow*) acquired in a more damaged building (photograph by Leucci)

Fig. 16 GPR depth slices related to the more damaged building shown in Fig. 14: **a** 37–54 cm depth; **b** 137–154 cm depth

Fig. 17 GPR depth slices related to another damaged building: **a** 51–72 cm depth; **b** 190–211 cm depth

header editing for inserting the geometrical information; (2) frequency filtering; (3) manual gain, to adjust the acquisition gain function and enhance the visibility of deeper anomalies; (4) customized background removal to attenuate the horizontal banding in the deeper part of the sections (ringing), performed by subtracting in different time ranges a "local" average noise trace estimated from suitably selected time–distance windows with low
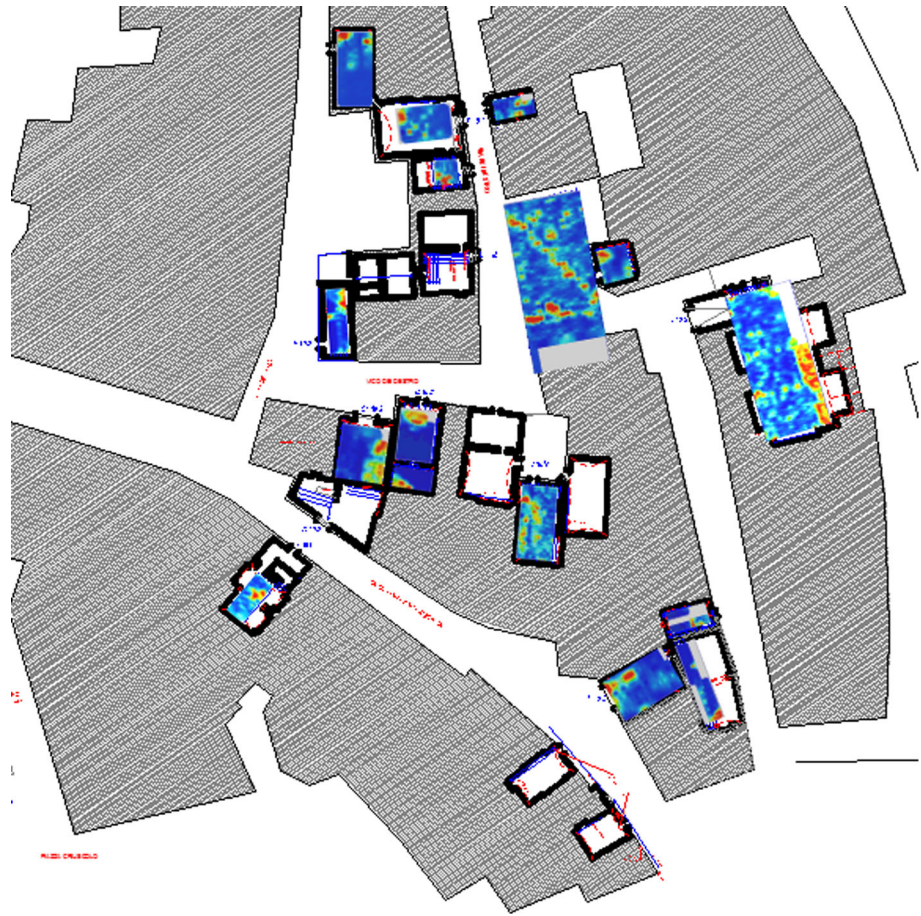
Fig. 18 GPR depth slices related to the whole surveyed area

signal content (this local subtraction procedure was necessary to avoid artefacts created by the classic subtraction of a "global" average trace estimated from the entire section, due to the presence of zones with a very strong signal); (5) estimation of the average electromagnetic wave velocity by hyperbola fitting; and (6) Kirchhoff migration, using a constant average velocity value of 0.07 m/ns. The migrated data were subsequently merged together into three-dimensional volumes and visualized in various ways in order to enhance the spatial correlations of anomalies of interest. A way of obtaining visually useful maps for understanding the plan distribution of reflection amplitudes within specific time intervals is the creation of horizontal time slices. These are maps on which the reflection amplitudes have been projected at a specified time (or depth), with a selected time interval (Conyers 2006). In a graphic method developed by Goodman et al. (2006), termed "overlay analysis", the strongest and weakest reflectors at the depth of each slice are enhanced with specific colours. This technique allows the linkage of structures buried at different depths. This represents an improvement in imaging because subtle features that are indistinguishable on radar grams can be seen and more easily interpreted. In the present work, the

time-slice technique has been used to display the amplitude variations within consecutive time windows of width $\Delta t = 5$ ns.

In order to define the depth of the anomaly zones, the electromagnetic (EM) wave velocity, using the characteristic hyperbolic shape of a reflection from a point source (diffraction hyperbola), was used.

Figure 15 shows one of the GPR processed profiles acquired in the more damaged building. The GPR profiles that were measured in the area (Fig. 15) show an hyperbolic-shaped reflection labelled C at the two-way travel time window between 10 and 20 ns. Its size is about 1.5 m, and the depth of the top is between 0.35 and 0.70 m (with an average electromagnetic wave velocity of 0.07 m/ns). The hyperbolic-shaped reflection labelled C was interpreted as a cavity.

In order to identify the depth evolution of buried structures, including their size, shape, and location, time slices were built (Fig. 16). The time slices show the normalized amplitude using a range defined by blue as zero and red as 1. In the slices ranging from 37 to 54 cm depth, relatively high-amplitude anomalies (labelled C, D, and P) are clearly visible. In the time slices ranging from 137 to 154 cm depth, other anomalies are visible (I and E), while the anomaly labelled P is again visible.

The anomaly "P" was interpreted as a well (in this point the profile crossed a known well), while anomalies C, D, I, and E that have similar shape and an inversion of wave polarity (Leucci et al. 2016) were interpreted as cavities.

Figure 17 shows time slices map related to another surveyed building. Also in this case the anomaly "P" was interpreted as a well, while anomaly "C" was interpreted as cavity.

In all surveyed areas, the GPR results allowed to highlight the presence of several anomalies (in particular, those in red colour in Fig. 18), related to buried critical zones. In such areas, in fact, instability events occurred, due to small voids, cavities and areas were previous artificial changes had been done. It can be noted that, as expected, in many houses the presence of wells and/or tanks, some of which partially filled with debris materials, was detected.

3 Conclusions

The proposed study allows the identification of hazard areas in the historical centre of Mesagne. For the studied area, data from stratigraphical information relative to 17 wells were collected. These data were integrated with geophysical data. This allowed the identification of the local geology, and particularly the depth of the groundwater table and the principal directions of the groundwater flow. The identification of the local geology (lithological classification) to determine subsoil physical characteristics related to the studied site was made.

The performed study demonstrates, one more time, the wide range of applicability of the geophysical methodologies. The results of the 3D ERT measurements showed the presence of a highly "disturbed" subsoil and a phase of adjustment still going on at the time of the measurements (March 2014). The SP data showed probable direction of flux of lose materials at the time of the prospecting. The GPR survey campaigns allowed to highlight the presence of several anomalies linked to buried critical zones.

According to the achieved results, it is possible to deem that the instability events have been caused by: (1) losses within both the water supply networks and the drainage systems. (2) The uncontrolled condition of several wells (in particular their high number and above

all their state of these wells had never been systematically monitored). (3) Rainwater that infiltrates into the subsoil. In particular, the flowing fluids can saturate the soil and reduce its mechanical resistance. Moreover, the infiltration of superficial runaway water, even in small quantity, can increase the foundation base plastic material quality, lowering the load capacity. Finally, indeed, also modern volumetric changes performed on some houses (e.g. perforation of load bearing walls) have made the structures more prone to damages, but this does not seem to be the main cause of the occurred problems.

References

Anderson MP, Woessner WW (1992) Applied groundwater modeling: simulation of flow and advective transport. Academic Press Inc, San Diego, p 381

Argote-Espino D, Tejero-Andrade A, Cifuentes-Nava G, Iriarte L, Farıas S, Chavez RE, Lopez F (2013) 3D electrical prospection in the archaeological site El Pahnu, Hidalgo State, Central Mexico. J Archaeol Sci 40:1213–1223

Aubanel EE, Oldham KB (1985) Fourier smoothing without the fast Fourier transform. Byte 10(2):207–218

Autorità di Bacino della Puglia (2006) Atto di indirizzo per la messa in sicurezza dei territori a rischio di cavità sotterranee. 7 pp [in Italian] Available at www.adb.puglia.it/public. Accessed 20 Nov 2015

Capizzi P, Martorana R, Messina P, Cosentino PL (2012) Geophysical and geotechnical investigations to support the restoration project of the Roman 'Villa del Casale', Piazza Armerina, Sicily, Italy. Near Surf Geophys 10(2):145–160. doi:10.3997/1873-0604.2011038

Carbonel D, Rodríguez V, Gutiérrez F, Mccalpin JP, Linares R, Roqué C, Zarroca M, Guerrero J, Sasowsky I (2014) Evaluation of trenching, ground penetrating radar (GPR) and electrical resistivity tomography (ERT) for sinkhole characterization. Earth Surf Process Landf 39(2):214–227. doi:10.1002/esp.3440

Carbonel D, Rodríguez-Tribaldos V, Gutiérrez F, Galve JP, Guerrero J, Zarroca M, Roqué C, Linares R, McCalpin JP, Acosta E (2015) Investigating a damaging buried sinkhole cluster in an urban area (Zaragoza city, NE Spain) integrating multiple techniques: geomorphological surveys, DInSAR, DEMs, GPR, ERT, and trenching. Geomorphology 229:3–16. doi:10.1016/j.geomorph.2014.02.007

Cataldo A, Persico R, Leucci G, De Benedetto E, Cannazza G, Matera L, De Giorgi L (2014) Time domain reflectometry, ground penetrating radar and electrical resistivity tomography:a comparative analysis of alternative approaches for leak detection in underground pipes. NDT E Int 62:14–28. doi:10.1016/j.ndteint.2013.10.007

Chavez G, Tejero A, Alcantara MA, Chavez RE (2011) The 'L-Array', a tool to characterize a fracture pattern in an urban zone: in expanded abstracts: near surface 2011. Eur As Geosci Eng 1:114–155

Ciaranfi N, Pieri P, Ricchetti G (1992) Note alla carta geologica delle Murge e del Salento (Puglia centromeridionale). Mem Soc Geol It 41(1988):449–460 **(With attached the Geological Map to scale 1:250.000)**

Cinque A, Patacca E, Scandone P, Tozzi M (1993) Quaternary kinematic evolution of the Southern Apennines. Relationship between surface geological features and deep lithospheric structures. Ann Geofis 36(2):249–260

Clavier C, Coates G, Dumanoir J (1977) Theoretical and experimental bases for the dual-water model for interpretation of shaly sands. In: Proceedings of the 52nd annual meeting, society of petroleum engineering, Denver, USA, Report SPE-6859-PA, preprint 16 pp

Colangelo G, Lapenna V, Perrone A, Piscitelli S, Telesca L (2006) 2D self potential tomographies for studying groundwater flows in the Varco d'Izzo landslide (Basilicata, southern Italy). Eng Geol 88(3):274–286. doi:10.1016/j.enggeo.2006.09.014

Conyers LB (2006) Innovative ground-penetrating radar methods for archaeological mapping. Archaeol Prospect 13(2):139–141

Gallipoli MR, Gizzi FT, Rizzo E, Masini N, Potenza MR, Albarello D, Lapenna V (2012) Site features responsible for uneven seismic effects in historical centre of Melfi (Basilicata, Southern Italy). Disaster Adv 5(3):125–137

Giannotta MT, De Giorgi L, Leucci G, Matera L, Persico R, Riccardi A (2015) Preventive archaeology: the emblematic case of Ruvo di Puglia, Italy. In: 8th international workshop on advanced ground penetrating radar (IWAGPR), 7–10 July 2015. Florence

Giudici M, Margiotta S, Mazzone F, Negri S, Vassena C (2012) Modelling hydrostratigraphy and groundwater flow of a fractured and karst aquifer in a Mediterranean basin (Salento peninsula, southeastern Italy). Environ Earth Sci 67:1891–1907

Goodman D (2013) GPR slice version 7.0 manual. http://www.gpr-survey.com. Accessed June 2013

Goodman D, Piro S (2013) GPR remote sensing in archaeology. Springer-Verlag ed., ISBN: 978-3-642-31856-6

Goodman D, Steinberg J, Damiata B, Nishimure Y, Schneider K, Hiromichi H, Hisashi N (2006) GPR overlay analysis for archaeological prospection. In: Proceedings of the 11th international conference on ground penetrating radar. CD-rom, Columbus, Ohio

Hill HJ, Shirley OJ, Klein GE (1979) Bound water in shaley sands—its relation to Qv and other formation properties. Log Anal 20(3):3–19

Juhasz I (1986) Assessment of the distribution of shale, porosity and hydrocarbon saturation in shaly sands. In: Transactions society professional well log analysts 10th European formation evaluation symposium, Ch. 15. Aberdeen, Scotland, paper AA

Leucci G (2015) Geofisica applicata all'archeologia e ai Beni Monumentali. Dario Flaccovio, Palermo pp 368, ISBN-978-88-98773-44-2

Leucci G, Negri S (2006) Use of ground penetrating radar to map subsurface archaeological features in an urban area. J Archaeol Sci 33:502–512. doi:10.1016/j.jas.2005.09.006

Leucci G, Negri S, Carrozzo MT, Nuzzo L (2002) Use of ground penetrating radar to map subsurface moisture variations in an urban area. J Environ Eng Geophys (JEEG) 7(2):69–77

Leucci G, Margiotta S, Negri S, Nuzzo L, Sansò P, Varola A (2003) Integrated geophisical, geological and geomorphological investigations for study the impact of agricultural activities on a complex karstic area. In: Proceedings del SAGEEP 2003 della environmental and engineering geophysical society. S Antonio (Texas, USA). 6–10 April 2003

Leucci G, Persico R, Soldovieri F (2007) Detection of Fracture From GPR data: the case history of the Cathedral of Otranto". J Geophys Eng 4:452–461

Leucci G, Masini N, Persico R, Soldovieri F (2011) GPR and sonic tomography for structural restoration: the case of the Cathedral of Tricarico. J Geophys Eng 8(3):S76–S92

Leucci G, Parise M, Sammarco M, Scardozzi G (2016) The use of geophysical prospections to map ancient hydraulic works: the Triglio underground aqueduct (Apulia, southern Italy). Archaeological Prospection, Published online in Wiley Online Library (wileyonlinelibrary.com) Doi:10.1002/arp.1541

Lowrie W (2007) Fundamentals of geophysics. Cambridge University Press, Cambridge

Malmström VH (1969) A new approach to the classification of climate. J Geogr 68(6):351–357. doi:10.1080/00221346908981131

Meiser P (1962) A method of quantitative interpretation of selfpotential measurements. Geophys Prosp 10(2):203–218. doi:10.1111/j.1365-2478.1962.tb02009.x

Paul MK (1965) Direct interpretation of self-potential anomalies caused by inclined sheets of infinite horizontal extensions. Geophysics 30(3):418–423. doi: 10.1190/1.1439596

Perrier FE, Petiau G, Clerc G, Bogorodsky V, Erkul E, Jouniaux L, Lesmes D, Macnae J, Meunier JM, Morgan D, Nascimento D, Oettinger G, Schwarz G, Toh H, Valiant MJ, Vozoff K, Yazici-Cakin O (1997) A one-year systematic study of electrodes for long period measurements of the electric field in geophysical environments. J Geomagn Geoelectr 49(11–12):1677–1696. doi:10.5636/jgg.49.1677

Pike JG (1964) The estimation of annual run-off from meteorological data in a tropical climate. J Hydrol 2(2):116–123. doi:10.1016/0022-1694(64)90022-8

Piscitelli S, Rizzo E, Cristallo F, Lapenna V, Crocco L, Persico R, Soldovieri F (2007) GPR and microwave tomography for detecting shallow cavities in the historical area of Sassi of Matera (Southern Italy). Near Surf Geophys 5(4):275–285. doi:10.3997/1873-0604.2007009

Sileo M (2011) Individuazione e caratterizzazione geologica, chimico-mineralogica e petrofisica di calcareniti tenere della Puglia e della Basilicata in relazione alle problematiche di provenienza e conservazione dei Beni Culturali. Ph.D. Thesis, University of Basilicata, Potenza, Italy (in Italian)

Tejero-Andrade A, Cifuentes G, Chavez RE, Lopez Gonzalez A, Delgado-Solorzano C (2015) ''L'' and ''Corner'' arrays for 3D electrical resistivity tomography: an alternative for urban zones. Near Surf Geophys 13:1–13. doi:10.3997/1873-0604.2015015

Telford WM, Geldart LP, Sheriff RE (1990) Applied geophysics. CambridgeUniversity Press, Cambridge

Tsokas GN, Kim JH, Tsourlos PI, Angistalis G, Vargemezis G, Stampolidis A, Diamanti N (2015) Investigating behind the lining of the Tunnel of Eupalinus in Samos (Greece) using ERT and GPR. Near Surf Geophys 13(6):571–583. doi:10.3997/1873-0604.2015012

Vichabian Y, Morgan FD (2002) Self potentials in cave detection. Lead Edge 21(9):866–871. doi:10.1190/1.1508953